

Improve Simulation of Plain Bearings in Dry and Mixed Lubrication Regime by Defining Locally Resolved Dry Friction Coefficients

C. Schneider^a, G. Wachtmeister^a, P. Klumpp^b, J. Halbhuber^a

^aInstitute of internal combustion engines, Schragenhofstreet 31, 80992 Munich, Germany,

^bAudi AG, Simulation mechanics powertraing, 85045 Ingolstadt, Germany.

Keywords:

Friction coefficient
Asperity contact
Mixed lubrication
Plain bearing simulation
Wear

ABSTRACT

Asperity friction is a main indicator for wear and heat conduction [1]. It occurs when thickness of oil film shrinks due to high load or slow speed. Friction is scientifically well known as long as it is dominated by laminar oil film effects. If film thickness shrinks, the friction coefficient depends mainly on surface properties. This inaccuracy is normally preceded in simulation by using friction coefficients defined by Coulomb's law [2].

To improve simulation results, the simulated friction moment was compared to measurement on a component test rig. Friction moment is produced on every square millimetre of the bearing surface, but can only be measured as an integral. Research findings show that measured results can't be met by using one global dry friction coefficient for the whole bearing surface, even though it is material dependent.

By introducing locally resolved and asperity pressure dependent dry friction coefficients, it was possible to adapt the simulated friction moment to measure one with a deviation of less than 5 percent. By means of simulation it was possible to develop locally resolved results based on integral measurements; and improve modelling the frictional state of mixed lubrication.

Corresponding author:

Carsten Schneider
Institute of internal combustion
engines TU Munich,
Schragenhofstreet 31,
80992 Munich, Germany.
E-mail: c.schneider@lvk.mw.tum.de

© 2015 Published by Faculty of Engineering

1. INTRODUCTION

Improvement of simulation technology in regions of a tribological system where asperity contact appears is the aim of this article. This state is called boundary lubrication and was introduced by Hardy in 1920s [3]. Therefore a very elementary test bench was built up to measure the friction moment of two plain

bearings. The simulation represents this test bench with its stiffness, the constant acting force, surface characteristics and material properties. Further the oil flow is calculated by elasto-hydrodynamic lubrication EHL what improves results shown by Gulzar [4]. The surface characteristics of the plain bearings were measured with a confocal microscope and introduced into the simulation model.

By comparing the measured friction moments with simulated ones, the integral friction coefficients of both systems were matched with an accuracy of better than 5 %. The local friction coefficient depends mainly on the asperity contact pressure and is calculated for every mesh grid in the simulation model.

2. STRATEGY

To calibrate simulation results and reach new knowledge about any kind of system, one of the best ways is to compare it with measurement results. For building up knowledge it is not expedient to do this at one of the most complex systems like a series internal combustion engine ICE. If the system is quite complex, there can be interactions between measured sizes which can't be split up into single effects. Further, there is often no possibility to simulate these interactions within an acceptable time and accuracy. Instead, it makes sense to build up an elementary component test bench and transfer the results to more complex systems.

The design criteria for the test bench used for this research is to produce a similar frictional state in the plain bearings as it appears in an ICE, even though there act much higher forces. The feasibility of this aim is based on the theory developed by Stribeck [5] and Sommerfeld [6] who defined the dimensionless characteristic number:

$$So = \frac{F_R \cdot \psi^2}{w \cdot d \cdot \eta \cdot \omega} \quad (1)$$

known as Sommerfeld number today. His theory claims that bearings with the same number share the same frictional state, even if they are very different in aspects of load, nominal clearance, bearing geometry, speed and oil viscosity.

To adjust the same Sommerfeld number at the test bench as it appears in an ICE, the boundary conditions defined in (1) have to be adapted accordingly. The radial force at the test bench is much lower than in an ICE, what can be compensated by a larger radial bearing clearance, a lower oil temperature and a lower angular velocity.

3. PLAIN BEARING TEST BENCH

3.1 Description

The test bench was built up to determine highly accurate measurement results of friction moment and friction coefficients for different bearing shell materials and surfaces.

Figure 1 shows a sectional view of the component test bench used for this research. A constant force of 2.6 kN presses against the shaft. This is realised with a roller cam follower to minimise its friction on the shaft, which would falsify the measurement results. The shaft is rotated by an electrical engine with rotational speeds between 1 and 1500 RPM. The bearing shells are placed symmetrically to the force and mounted in hydrostatic bearings. Between shaft and shell occurs friction which acts on the bedding, where the shell is fixed. Due to the friction moment, the bedding would rotate, what is prevented by load cells which measure this moment. The moment cannot be transmitted to the base due to the hydrostatic bearing which is nearly frictionless if no rotation appears. The rotational degree of freedom of the bedding is locked by the two load cells.

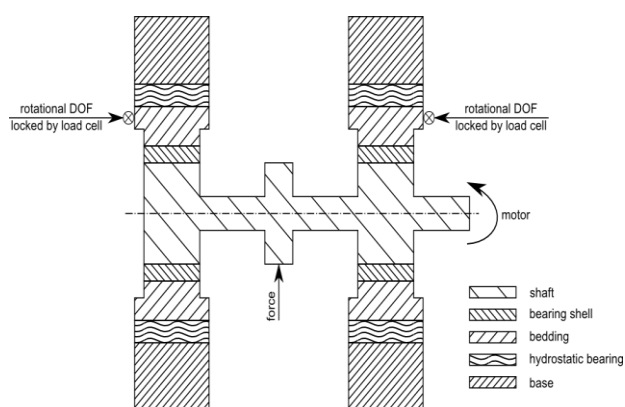


Fig. 1. Sectional view of plain bearing test bench.

To ensure that the plain bearings get enough oil, the supply is realised by bores with a diameter of 6 mm in the lower part. Used is a SAE 5W-30 oil and the measurements are made at a temperature of 85 degree Celsius. The oil supply pressure is set to 3.4 bar.

The researched shell is an aluminium alloy bearing with a steel backing. For the aluminium bearing layer the material properties are well known which is later important for the

simulation. For all studies, the same shaft made of steel was used.

3.2 Measurement Results

In order to examine the regions with high asperity contact pressure, extremely low rotational speeds have to be measured. This is realised by coast down and run-up experiments between 0 and 1500 RPM. To reach surface topographies comparable to those in an ICE, the rotational speed was kept at 20 RPM for a longer time to abrade the bearing shell. During the whole tests, the friction moment, temperatures at five positions, oil volume flow and rotational speed are measured. With these results a comparison to simulation can be performed.

To prove the influences of shaft wear and reconstructions because of changing the bearing shell, a reproducibility test was made. Two kinds of bearing shells were measured at the beginning and at the end of the experiment schedule, with the results shown in Fig. 2.

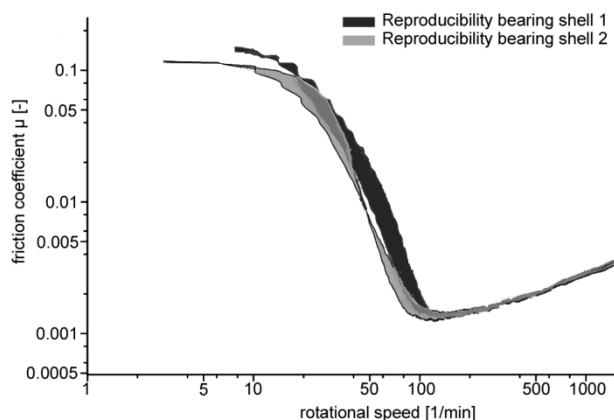


Fig. 2. Reproducibility of measurement results.

For both bearing shells, there are only minimal deviations between the friction coefficients inferred from friction moment at the beginning and at the end of the experiment schedule. This verifies a high reproducibility. On the other hand, the difference between the friction coefficients of bearing shell 1 and bearing shell 2 can clearly be seen in the mixed friction range. Consequently the measurement accuracy and the ability to measure the influence of shell surfaces and its material is proved.

Furthermore this study shows that the friction coefficients for these two bearing shells are

identical at rotational speeds higher than 100 RPM. This clearly illustrates that at higher speeds from this point on, the surface and material of the shell has no significant influence. Here the oil film is thick enough and hydrodynamic effects dominate this system.

The reproducibility is very good and proofs reliable measurement results. The influence of the bearing shell materials, their surfaces and the running-in effects are clearly represented and eligible to calibrate simulation parameters.

4. SIMULATION

4.1 Approximation of surface topography

The surface topographies of the bearing shells and the shaft influence the oil flow between the summits and the appearing asperity contact pressure, which themselves are important to identify areas with mixed friction.

Simulation tools can only handle numerical solvable equations. Due to this reason, the real surface topographies have to be transformed and simplified.

A refined model with one of the best known approximations invented by Greenwood and Tripp, was chosen in this case to get as realistic results as possible [7,8]. With this approximation the asperity contact pressure and the regions where it appears can be calculated, subject to the surface roughness follows a Gaussian distribution curve, as is the case.

For the oil flow between shaft and shell the Patir and Cheng model was chosen [9,10]. Oil flow factors are determined to adjust Reynold's equation for radial and axial oil flow depending on the surface topography and its orientation with this model [11].

The bearing shells and the shaft surfaces are measured by a confocal white light microscope with a resolution of 1.6 micron per pixel. The measured area is 800 times 800 micron, and 9 pictures are put together by stitching yielding a surface area of 4 square millimetres. The Greenwood and Tripp formula to calculate asperity contact pressure [7] contains a lot of variables like summit radius, summit density

and mean summit height, but all of them can be calculated based on the three dimensional measured real surfaces.

$$P_{Asperity} = \frac{16}{15} * \sqrt{2} * \pi * E' * \beta^{1,5} * \eta^2 * \sigma^{2,5} * F_{\frac{5}{2}} * \frac{d}{\sigma} \quad (2)$$

This makes the approximation exact enough to get realistic asperity contact pressure and oil flows.

4.2 Model

The tool chosen for this project is Excite™ Power Unit from AVL List GmbH as it supports elasto hydrodynamic (EHD) joint simulation, the effect of temperature on oil viscosity and its influence on the asperity contact. The EHD simulation is necessary to consider the elastic deformation of the shaft and the bearing shell [12] which improves the simulation results especially in the observed area of asperity contact. Thanks to the simple test bench, there are only few components in simulation model. This is important in order to get as few variables as possible and allows fast comprehensive parameter studies as of simulation times are shorter than two hours.

The component test bench housing and the shaft are represented by FEM models with their stiffness and geometry. The bearings can be modelled by a center-to-surface (CTS) or surface-to-surface (STS) contact. For CTS the shafts stiffness is reduced to 7 nodes per bearing in the rotation axis, for STS every surface node in this area is kept, what rises simulation time from 2 to 20 hours. The results generated with STS didn't show any significant improvement in comparison to CTS, so the shorter simulation time was chosen.

4.3 Results

The theory from Sommerfeld was assumed to be correct. To control this, the boundary conditions which influence the Sommerfeld number are examined. The radial force, the dynamic oil viscosity, the velocity and the bearing dimensions are constant in this system. Therefore the clearance has to be constant too, otherwise the Sommerfeld number is not valid for the whole bearing surface, but only for this part of the bearing where the real and the

nominal clearance value of 35 microns are the same.

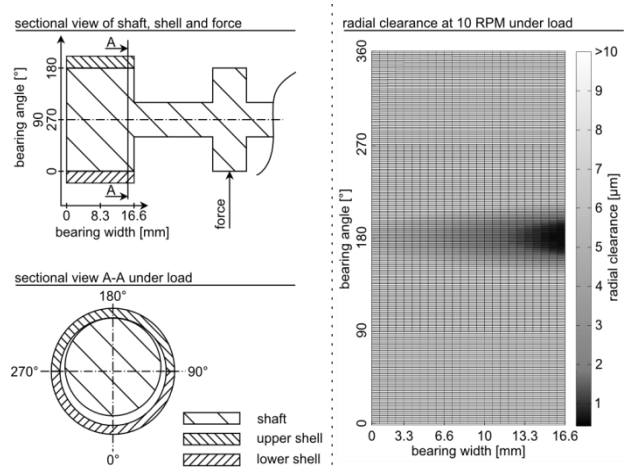


Fig. 3. Radial clearance under load at 10 RPM.

To proof this, the first simulation results shown in Fig. 3 are analysed. The clearance is not constant at every point of the shell, what makes us doubt this theory. What was not considered by Sommerfeld when he developed this theory is the shaft's deflection. Even with the low radial force of 2600 Newton acting at this test bench the shaft can't be assumed as rigid. Caused by its deflection, the shaft is pressed against the shell in the area around 180 degree bearing angle. In these regions the clearance goes closely to zero, whereas the maximum from 0 to 90 and 270 to 360 degree is more than 80 microns. Therefore the Sommerfeld number has to be a function dependent on the bearing width position.

The aim to hit every frictional state that appears in an ICE at the test bench, what was argued by Sommerfelds theory, has to be questioned. But if the bearing surface is split up in many small parts, the Sommerfeld number is applicable for each of these slices.

Further analysed was the friction coefficient determined in simulation which approximately should look like the curve shown in Fig. 2. To illustrate the disparity, measurement and simulation results are compared in Fig. 4. Obviously the simulation does not correspond to the measurement, even though the asperity pressure, ratio and oil flow are calculated by using the values gained from three dimensional measured surfaces. The dry friction coefficient first entered was 0.03. To coincide with measurement it is too small for low rotational

speed and too high for more than 30 RPM. Changing the constant friction coefficient to 0.01 or 0.05 only moves the curve parallel and doesn't improve simulation results. Nevertheless it is retained to the assumption that the results from Greenwood and Tripp and Patir and Cheng are realistic. Assuming that the main source of error is the entered dry friction coefficient, this magnitude is closely investigated.

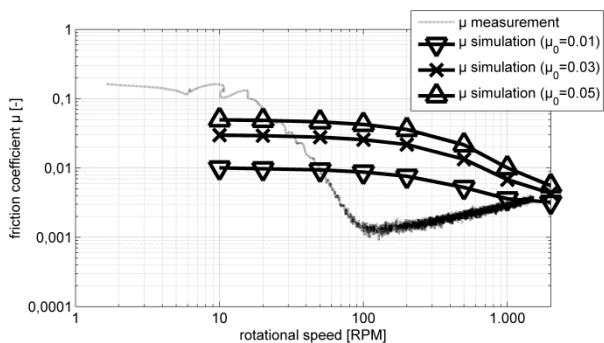


Fig. 4. Friction coefficients measurement and simulation.

During further investigations it was observed, that the simulation tool calculates with the entered dry friction coefficient at every node

asperity contact pressure appears. No matter if it is just 1 Pascal or 100 Megapascal, the friction coefficient is always the same as can be seen in Fig. 5. This approach obviously does not lead to realistic simulation results.

The idea which resolves this dilemma is depicted in Fig. 6. The asperity contact pressure behaves qualitatively like the clearance height shown in Fig. 3. In the area the shaft deflects, edge girder occurs and the asperity contact pressure rises. As illustrated in Fig. 6, for this test bench the contact occurs in the region of 180 degree bearing angle and bearing width of 16.6 millimetres. For this area, much higher dry friction coefficient than the constant one of 0.03 has to be defined. In contrast 0.03 is too big in transition areas of lower asperity pressure.

To proof this approach and analyse the exact distribution of locally dissolved friction coefficients, the variable parameters to calculate them are varied until the simulated and measured friction moment fit together.

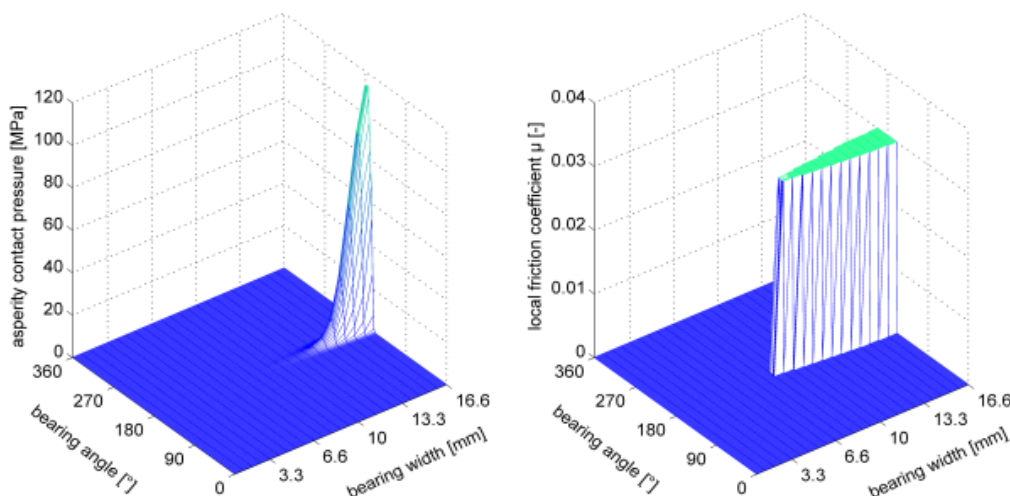


Fig. 5. Asperity contact pressure and constant friction coefficient.

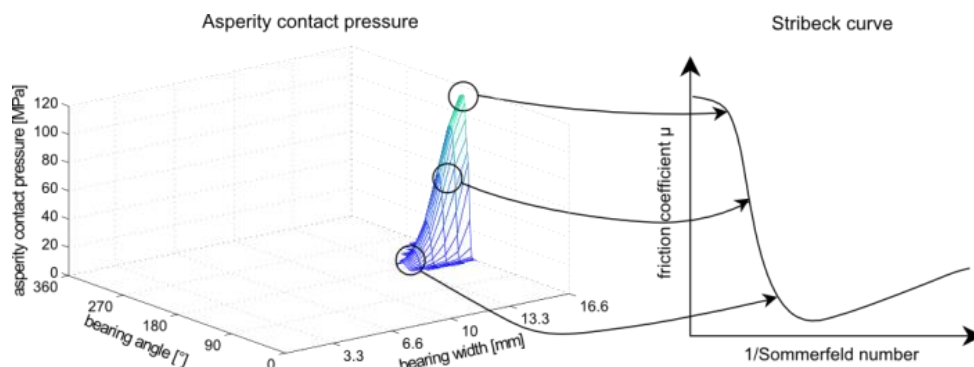


Fig. 6. Idea of locally dissolved friction coefficient.

5. COMPARISON: MEASUREMENT WITH SIMULATION

5.1 Function to calculate a local asperity friction coefficient

The one measured friction coefficient per operating point is a midpoint over the whole surface. It locally varies in a very large range as there are regions where pure hydrodynamic appears and some with mainly asperity contact. The reason is the elastic deformation of the shaft. In a specific bearing shell at a constant rotational speed with a constant force, nearly every point on the Stribeck curve is represented. In areas with high asperity contact pressure the mixed lubrication part of the curve is met, on those without asperity contact pressure the hydrodynamic one is met.

Simulation results gained by using a constant friction coefficient fail to describe the measured friction, as can be seen in Fig. 4. To improve simulation, a numerical solvable equation which defines friction coefficients dependent from asperity contact pressure has to be defined.

A suitable function was found within AVL Excite called "Lubricated asperity friction and wear" LAFW [13]:

$$\mu_{LAFW} = \mu_0 * A^{-\sqrt{B * L_N}} + C * r_c * L_N * (1 - A^{-\sqrt{B * L_N}}) \quad (3)$$

This equation defines local friction coefficients dependent on the parameters A , B , C and physical properties merged in L_N .

This function is implemented in a manner that it influences the calculation of friction moment and power losses only where asperity contact appears. In regions of pure hydrodynamic the Reynolds equation is not influenced by this. The first term of the sum represents the friction coefficient for summits in contact. The second term represents the lubricant flow between the summits.

Observing measurement results, μ_0 was chosen equal to the maximum value of the measured Stribeck curve, in this case 0.16. The aim to represent measured values did not work very well with this parameterisation as shown in Fig. 7.

A factor 'H' is introduced to enable the function to reach higher maximum friction coefficients, and the constant 'A' was replaced by Euler's number to form an exponential function:

$$\mu_{local} = H * \mu_0 * e^{-\sqrt{B * L_N}} + C * r_c * L_N * (1 - e^{-\sqrt{B * L_N}}) \quad (4)$$

An optimized match between measurement and simulation, shown in Fig. 7, was obtained for a value of 14 for 'H'. This can be interpreted as a local maximum friction coefficient of $14 * 0.16 = 2.24$.

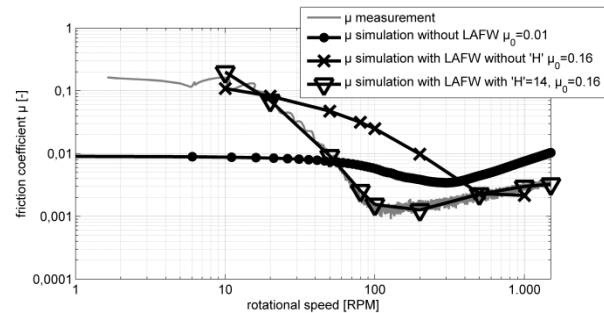


Fig. 7. Comparison of integral friction coefficients.

The product of $H * \mu_0$ is the friction coefficient which would appear in the theoretical case, that the whole bearing shell runs in uniform asperity contact with an asperity contact ratio of $r_c = 1$. In this case, there is no hydrodynamic pressure neither oil flow between the summits at all. Consequently the second term in (4) disappears. The parameters B and C depend on the shell material and surface. The process to define them is explained in the next chapter.

The Lubrication number, shortened with L_N in this function is a normalised index like the Sommerfeld number used to characterise a local friction state:

$$L_N = \frac{\eta * \Delta v}{P_{Asp} * L_S} \quad (5)$$

Included in this formula are, apart from the asperity contact pressure, the dynamic viscosity of the oil, the speed difference between the shaft and the shell and a characteristic length which depends on the surface topography.

5.2 Adjustment of parameters with measurement results

The main aim of the optimisation process is to split up the integrated, measured friction

moment into local friction coefficients. For this the measured friction moment is compared to the simulated, because one main influence on this value is the friction coefficient:

$$M_{R,Measurement} \stackrel{def}{=} M_{R,Simulation} = r_{Bearing} * \int_0^x \int_0^y (\tau_{Hyd}(x,y) + \tau_{Asp}(x,y)) \delta y \delta x \quad (6)$$

$$\tau_{Asp}(x, y) = P_{Asp,Simulation}(x, y) * \mu_{local}(x, y) \quad (7)$$

The friction moment is calculated in simulation by multiplying bearing radius with the integral of hydrodynamic and asperity shear stress (equitation 6). Accuracy is limited for the hydrodynamic part by the oil model used in simulation. Here a model from Vogel/Barus/Cross is used, which takes into consideration the change of dynamic viscosity by temperature, pressure and shear rate [14]. This is one of the most exact models and simulates this part of shear stress accurately. The asperity shear stress is resolved more detailed to see the particular influences (equitation 7).

The asperity pressure p_{Asp} is calculated by the Greenwood/Tripp (GT) model. The summits of the three dimensional measured surfaces are approximated by paraboloids also defined by GT. By supposing the accuracy of GT is exact enough, the only variable to fit simulation results to measurements is the local friction coefficient μ_{local} .

The parameters H , B and C of the function to calculate μ_{local} were optimised with Matlab™ to match the measurement results at every rotational speed. Used was a optimisation algorithm that minimizes the mistake to a minimal root square [15].

5.3 Results for local asperity friction coefficient

Comparing measurement with simulation and optimising the function for a local asperity friction coefficient gives a result for every mesh grid. The maximum is defined by $H * \mu_0$ in the μ_{local} -function, which is much higher than $\mu_0 = 0.16$ measured at the test bench. The results for 10, 20, 50 and 100 RPM are shown in Fig. 8. It is important to remember that these slow rotational speeds depict every locally dissolved Sommerfeld number of an turbocharged ICE. Equally the engine start and stop is represented, what underlines the technical relevance of this observation.

For the regarded bearing shell, the maximum asperity friction coefficient is 0.24. This is higher by a factor of 1.5 compared to measured integrated friction coefficient.

Full hydrodynamics formed at 100 RPM and higher, what meets measurement results explained above. With a constant friction coefficient there would still be asperity contact left till 500 RPM as can be seen in Fig. 7.

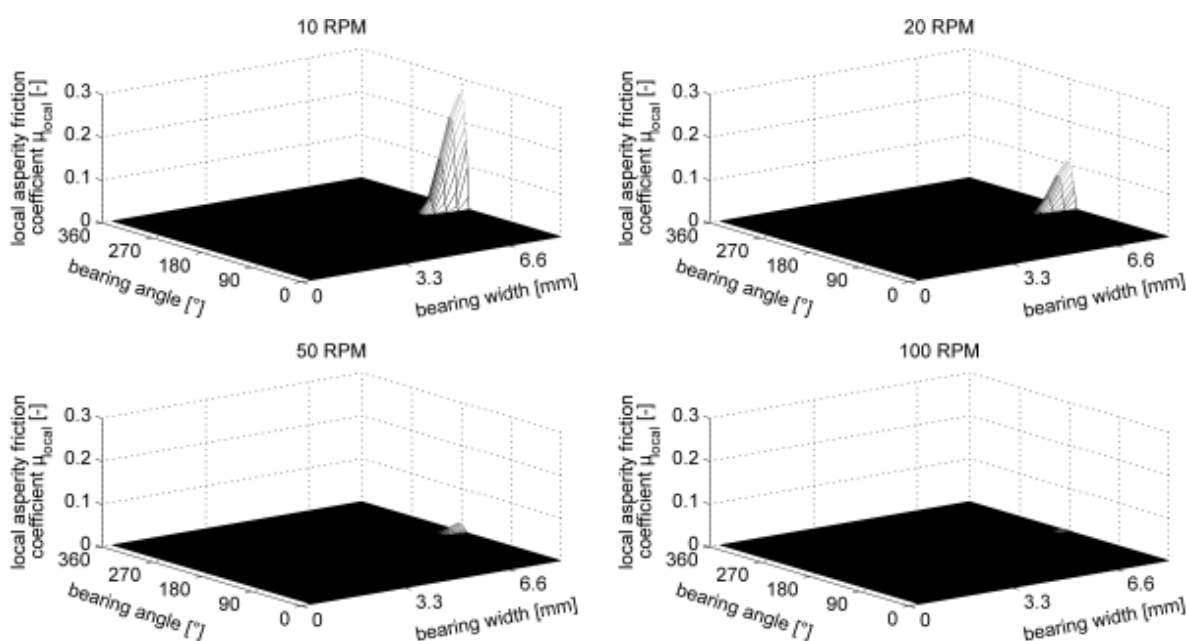


Fig. 8. Asperity friction coefficient at different rotational speed.

6. ACHIEVED IMPROVEMENT BY USING LOCALLY DISSOLVED FRICTION COEFFICIENT

To demonstrate the improvements made by using a local friction coefficient, Stribeck curves of measurement and simulation results are shown in the lower part of Fig. 9. The shown friction coefficients are the integral over the whole bearing surface including rising hydrodynamic with higher rotational speed. In simulation with a constant friction coefficient an experience based value of 0.03 was used.

This figure illustrates that a constant friction coefficient is the main source of error for simulation. As can be seen in the upper two diagrams of Fig. 5a, there is almost no difference between 10 RPM and 100 RPM for the reasons explained above. This is also reflected in the Stribeck curve, which is horizontal up to 100 RPM and does not coincide with measurement results. For rotational speeds up

to 30 RPM the integrated friction coefficient is too low, for higher speeds too high.

In contrast to the constant friction coefficient, the local one falls from a maximum at 10 RPM to almost zero at 100 RPM as can be seen in the two diagrams in the middle of Fig. 9. This behaviour represents exactly the measured Stribeck curve and improves simulation results.

The friction coefficient used in simulation strongly influences many technical interesting results like friction power loss, temperatures appearing inside the bearing shell and oil. The asperity friction power loss for example is calculated by:

$$\begin{aligned} \text{AsperityFrictionPowerLoss} &= \\ &= \mu_{\text{local}} * P_{\text{Asperity}} * S * \Delta v \end{aligned} \quad (8)$$

In order to emphasise the described influence, simulated asperity friction power loss results for constant and locally dissolved friction coefficients are shown in Fig. 10.

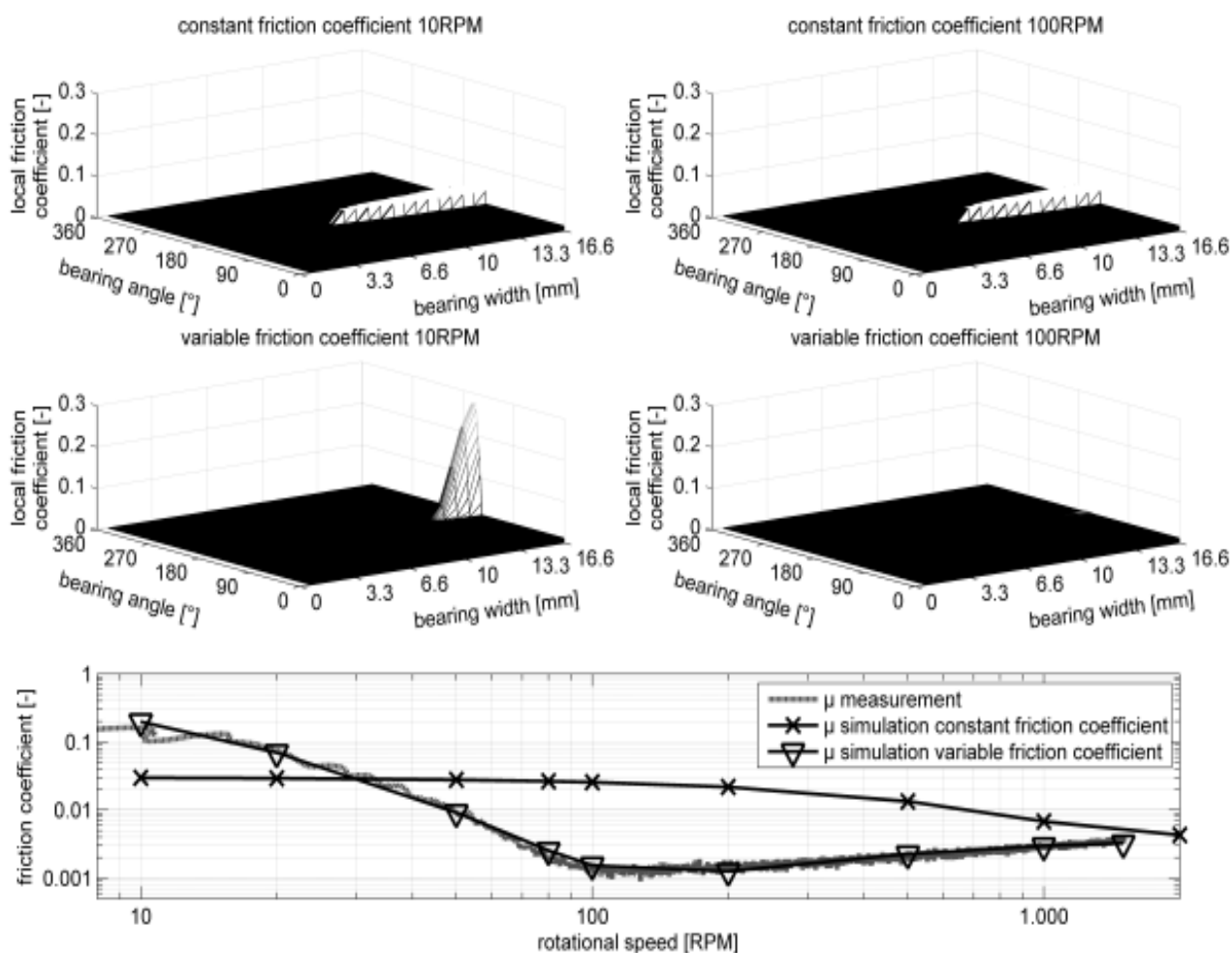


Fig. 9. Comparison of simulation results with and without local friction coefficients.

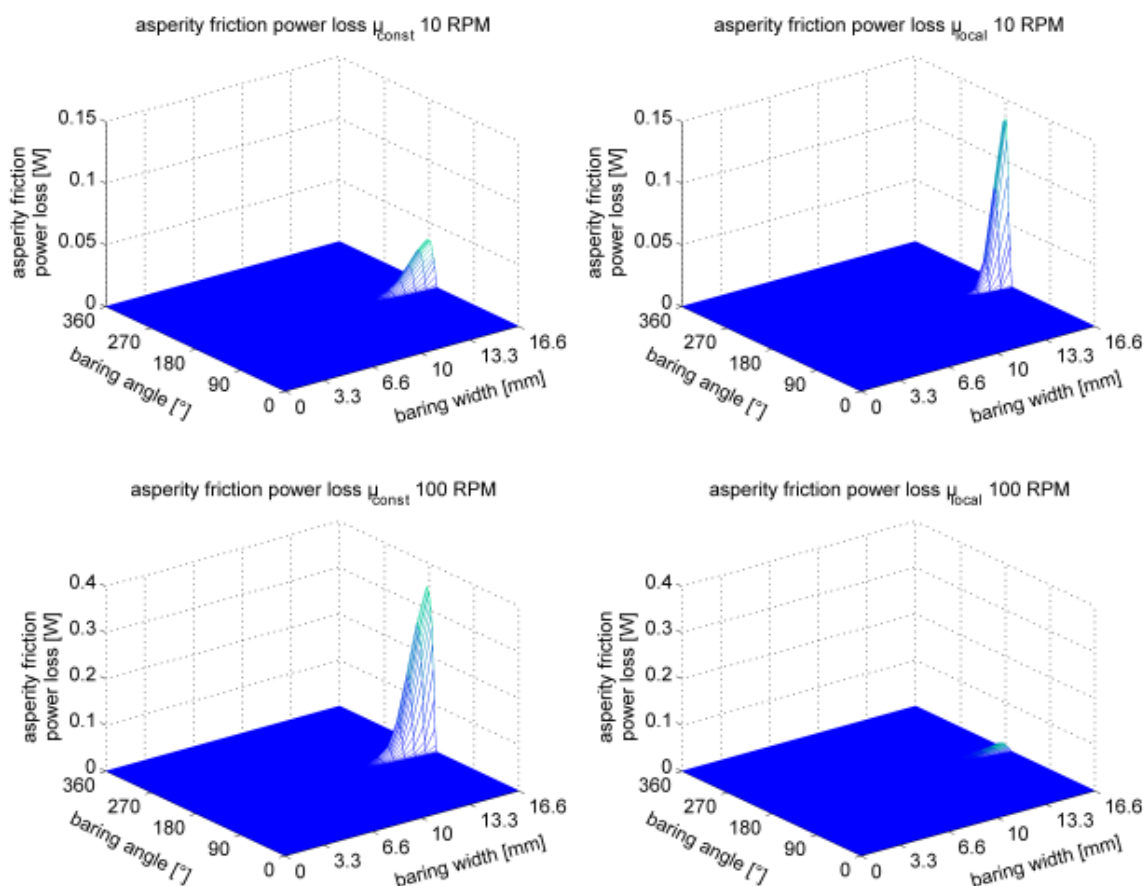


Fig. 10. Comparison of asperity friction power loss.

There is not a linear correlation between friction coefficient and asperity friction power loss. The value of a locally dissolved friction coefficient depends on the asperity pressure acting on each point. The asperity friction power loss is the product of friction coefficient and asperity pressure. For high asperity pressures there is consequently a high friction coefficient, what makes the influence almost quadratic. Within a bearing with edge girder, power loss is concentrated to a very small area, even more concentrated than the asperity contact pressure.

7. CONCLUSION

Quantitative simulation of friction power loss in plain bearings with high asperity contact ratio is not possible if a constant friction coefficient is used for the whole surface. It varies strongly, depending mainly on the asperity contact pressure, and is successfully modelled with the function for a local friction coefficient. The peak values of this function can reach unfamiliar numbers > 1 .

The asperity contact pressure itself can be calculated close to reality by using 3D real surface measurements and the classical models for approaching surfaces (Greenwood and Tripp) and oil flow (Patir and Cheng).

Future work will show whether the LAFW function parameters H , B and C can be generalized for certain classes of bearing shells. If this is possible, predictive simulations can be done just knowing the material and the surface topography of the bearing, and test bench calibration is necessary a few times only.

Furthermore, the outlined procedure can be applied to engine subsystems with multiple bearings like camshafts and crankshafts.

REFERENCES

- [1] S. Liu, Q. Wang, 'A three-dimensional thermomechanical model of contact between nonconforming rough surfaces', *ASME, Journal of Tribology*, vol. 123, no. 1, pp. 10, 2001.

- [2] W. Magie, *A source book in physics*. Cambridge: Harvard University Press, 1963.
- [3] W. Hardy and I. Doubleday, 'Boundary Lubrication. The Paraffin Series', *Proceedings of the Royal Society A: Mathematical, Physical and Engineering Sciences*, vol. 100, no. 707, pp. 550-574, 1922.
- [4] M- Gulzar, S.A. Qasima and R.A. Mufti, 'Modelling the Rough Piston Skirts EHL at a Small and a Large Radial Clearance in the Initial Engine Start Up', *Tribology in Industry*, vol. 35, no. 4, 2013.
- [5] R. Stribeck, *Die wesentlichen Eigenschaften der Gleit- und Rollenlager*. Berlin: Springer, 1903.
- [6] N. Petrow, O. Reynolds, A. Sommerfeld und A. G. M. Michell. *Abhandlungen über die hydrodynamische Theorie der Schmiermittelreibung*. Herausgegeben von L. Hopf, Aachen. Mit 45 Textfiguren. Ostwald's Klassiker der exakten Wissenschaften Nr. 218. Akademische Verlagsgesellschaft m. b. H., Leipzig 1927. 227 S. Preis 5,60 M', *ZAMM - Zeitschrift für Angewandte Mathematik und Mechanik*, vol. 8, no. 2, pp. 155-155, 1928.
- [7] J. Greenwood and J. Tripp, 'The contact of two nominally flat rough surfaces', *ARCHIVE: Proceedings of the Institution of Mechanical Engineers 1847-1982 (vols 1-196)*, vol. 185, no. 1970, pp. 625-634, 1970.
- [8] A. Mitra, P. Sahoo and K. Saha, 'A Multi Asperity Model of Contact between a Smooth Sphere and a Rough Flat Surface in Presence of Adhesion', *Tribology in Industry*, vol. 33, no.1, 2011.
- [9] N. Patir and H. Cheng, 'Application of Average Flow Model to Lubrication between Rough Sliding Surfaces', *J. Lub. Tech.*, vol. 101, no. 2, p. 220, 1979.
- [10] N. Patir and H. Cheng, 'An Average Flow Model for Determining Effects of Three-Dimensional Roughness on Partial Hydrodynamic Lubrication', *J. Lub. Tech.*, vol. 100, no. 1, p. 12, 1978.
- [11] Q.J. Wang and Y.-W. Chung, *Encyclopedia of Tribology - Reynolds equation*, Springer Science and Business Media, New York, 2013.
- [12] M. Steinbatz, *EHD-contact in engine simulations using a modal force approach in commercial multi-body simulation software*. London: SAE International, 2010.
- [13] AVL Advanced Simulation Technologies: *Power Unit Theory guide for version 2013.1*, AVL™, 2013.
- [14] S. Bukovnik, G. Offner, V. Čaika, H. Priebsch and W. Bartz, 'Thermo-elasto-hydrodynamic lubrication model for journal bearing including shear rate-dependent viscosity', *Lubrication Science*, vol. 19, no. 4, pp. 231-245, 2007.
- [15] A. Björck, *Numerical methods for least square problems*. Amsterdam: SIAM, 1996.